The EMBO Journal Vol.16 No.15 pp.4760–4769, 1997

Crystal structure at 1.2 Å resolution and active site mapping of *Escherichia coli* peptidyl-tRNA hydrolase

Emmanuelle Schmitt, Yves Mechulam, Michel Fromant, Pierre Plateau and Sylvain Blanquet[1]

Laboratoire de Biochimie, Unité de Recherche Associée No. 1970 du Centre National de la Recherche Scientifique, Ecole Polytechnique, F-91128 Palaiseau cedex, France

[1]Corresponding author

Peptidyl-tRNA hydrolase activity from *Escherichia coli* ensures the recycling of peptidyl-tRNAs produced through abortion of translation. This activity, which is essential for cell viability, is carried out by a monomeric protein of 193 residues. The structure of crystalline peptidyl-tRNA hydrolase could be solved at 1.2 Å resolution. It indicates a single α/β globular domain built around a twisted mixed β-sheet, similar to the central core of an aminopeptidase from *Aeromonas proteolytica*. This similarity allowed the characterization by site-directed mutagenesis of several residues of the active site of peptidyl-tRNA hydrolase. These residues, strictly conserved among the known peptidyl-tRNA hydrolase sequences, delineate a channel which, in the crystal, is occupied by the C-end of a neighbouring peptidyl-tRNA hydrolase molecule. Hence, several main chain atoms of three residues belonging to one peptidyl-tRNA hydrolase polypeptide establish contacts inside the active site of another peptidyl-tRNA hydrolase molecule. Such an interaction is assumed to represent the formation of a complex between the enzyme and one product of the catalysed reaction.

Keywords: crystalline structure/esterase/peptidyl-tRNA/translation

Introduction

In the course of the elongation of a protein, peptidyl-tRNAs can dissociate prematurely from the ribosome, resulting in abortive polypeptide chain termination (Menninger, 1976, and references therein). Such a disruption of translation depends heavily on the tRNA involved, with $tRNA^{Lys}$ dissociating 30-fold more frequently than $tRNA^{Gly}$ for instance (Menninger, 1978). The peptidyl-tRNAs which accumulate in the cytoplasm are toxic for the cell, by either impairing the initiation of translation or slowing down protein synthesis through a limitation of the corresponding tRNAs (Chapeville *et al.*, 1969; Menninger, 1976; Atherly, 1978).

Activities capable of recycling peptidyl-tRNAs into tRNAs have been characterized in prokaryotes (Cuzin *et al.*, 1967; Kössel and RajBhandary, 1968; Kössel, 1969), in yeast (Kössel and RajBhandary, 1968; Jost and Bock, 1969) and in higher eukaryotes (Gross *et al.*, 1992a,b). In bacteria and yeast, this activity, carried out by peptidyl-tRNA hydrolase (PTH), is an esterase one. In rabbit reticulocytes, the mechanism differs, with peptidyl-AMP and tRNA-CC being the products of the reaction (Gross *et al.*, 1992a).

Thermosensitive *Escherichia coli* mutants mapping in the *pth* gene were isolated, thereby indicating the essential character of PTH (Atherly and Menninger, 1972; Garcia-Villegas *et al.*, 1991; Menninger and Coleman, 1993). With such mutants, the rate of killing at various non-permissive temperatures correlates with the extent of accumulation of peptidyl-tRNA (Menninger, 1979). In addition, the thermosensitive character of the mutants could be accentuated by antibiotics believed to cause premature termination of translation (Menninger and Coleman, 1993). Recently, it was established that a pth^{ts} strain is cured upon overexpression of $tRNA^{Lys}$, a tRNA particularly prone to premature dissociation from the ribosome (Heurgue-Hamard *et al.*, 1996).

The substrate specificity of *E.coli* PTH depends on both the peptidic and the nucleotidic moieties of the substrate (Kössel and RajBhandary, 1968; Shiloach *et al.*, 1975a). N-blocked aminoacyl-tRNAs are the shortest substrates of the enzyme, with K_m values in the micromolar range and k_{cat} values in the s^{-1} range (Schulman and Pelka, 1975; Shiloach *et al.*, 1975a; Dutka *et al.*, 1993). Whereas unaminoacylated tRNAs behave as competitive inhibitors, no measurable inhibition of PTH could be evidenced with free peptides at concentrations of up to 1 mM (Shiloach *et al.*, 1975a). However, comparison of substrate tRNAs carrying peptides of various lengths showed that extension of the peptidic moiety to up to four residues decreased the K_m by nearly 5-fold, while the k_{cat} was improved by a factor of 10 (Shiloach *et al.*, 1975a). This result suggests a contribution to the efficiency of hydrolysis of additional residues beyond the amino acid esterified to tRNA.

PTH is usually assayed with N-blocked aminoacyl-tRNAs (Kössel, 1969). Notably, however, formyl-methionyl-$tRNA_f^{Met}$ is resistant to attack by PTH (Kössel and RajBhandary, 1968; Schulman and Pelka, 1975). This behaviour enables the cell to keep this tRNA intact for translation initiation. The main structural feature accounting for the resistance is the absence of a strong base pairing at position 1–72 in the prokaryotic initiator tRNA (Schulman and Pelka, 1975; Dutka *et al.*, 1993). Interestingly, this feature of tRNA is also the major determinant allowing the reaction of methionyl-$tRNA_f^{Met}$ transformylase (Lee *et al.*, 1991; Guillon *et al.*, 1992). Therefore, the same identity element at the top of the acceptor stem of $tRNA_f^{Met}$ accounts for both formylability and resistance to PTH. The rate of hydrolysis of an N-blocked aminoacyl-tRNA by *E.coli* PTH also depends markedly on the 5′-phosphate of the substrate (Schulman and Pelka, 1975). It is likely that the requirement for base pairing at position

1–72 in the tRNA substrate is related to the necessity for precisely adjusting the position of this phosphate group within the active site of PTH.

To understand the structure–function relationships of PTH, the determination of its three-dimensional folding is of particular interest. The enzyme previously was crystallized in a form suitable for X-ray studies (Schmitt *et al.*, 1997). The present work describes the corresponding three-dimensional structure at 1.2 Å resolution.

Results and discussion

Structure resolution

Orthorhombic crystals of PTH having unit cell parameters of a = 47.2 Å, b = 63.6 Å, c = 62.6 Å and belonging to space group $P2_12_12_1$ were obtained as described (Schmitt *et al.*, 1997). The structure of PTH was solved from these crystals by multiple isomorphous replacement (MIR) using four derivatives. The final refined model of PTH includes all 193 residues of the enzyme. A total of 181 water molecules have been placed in the asymmetric unit. The crystallographic *R*-factor is 19.6% for 50 645 unique reflections between 8.0 and 1.2 Å (2σ cut-off). The free *R*-factor (Brünger, 1992b), calculated with the remaining 3276 reflections, not included in refinement, is 21.5%. The root mean square (r.m.s.) co-ordinate error was estimated to be ~0.15 Å (Luzatti, 1952). The model has a good geometry, with an r.m.s. deviation from ideal geometry of 0.008 Å for bond lengths and 1.6° for bond angles. All residues, except Phe66, have φ and ψ angles within the allowed regions of the Ramachandran plot, with 95.6% in the most favoured region. The average temperature factor is 17.0 $Å^2$ for all protein atoms and 33.9 $Å^2$ for solvent atoms.

Overall structure

PTH behaves in solution as a monomer (Kössel, 1969). The crystals used contain one molecule in the asymmetric unit, and the fraction of the unit cell occupied by protein atoms is 54.5%. The enzyme is composed of a single α/β globular domain (Figure 1A). A central mixed β-sheet is formed by two antiparallel strands (β2 and β3) followed by four parallel strands (β4, β1, β5 and β7) and one antiparallel strand (β6). This β-sheet is twisted by ~90°, and is surrounded by five α-helices. Helices α2 and α3 are located on the same side as the C-terminal part of strand β2, whereas helices α1, α5 and α6 are located on the opposite side, near the N-terminal part of the β2 strand. Finally, helix α4 is located above a crevice, at the C-end of the four central parallel strands (Figure 1A).

A schematic representation of the topology of the enzyme is shown in Figure 1A. It resembles one subunit of the homotrimeric purine nucleoside phosphorylase from calf spleen (Koellner *et al.*, 1997; C.Mao, M.Zhou, S.Ealick, A.A.Frederov and S.C.Almo, submitted, PDB entry 1PBN). The β-strands and α-helices of PTH, with the exception of α1, α4 and α6, have counterparts in the purine nucleoside phosphorylase. These secondary structure elements have the same organization along the two amino acid sequences. Superimposition of the two structures yields an r.m.s. deviation of 2.07 Å for 94 pairs of Cα compared. The phosphorylase structure, however, shows two additional strands such that the global fold is a nine-stranded mixed β-barrel (Koellner *et al.*, 1997). Because of this marked difference and the lack of relationships between the activity of the phosphorylase and that of the PTH, this comparison was not investigated further.

Comparison of the structure of PTH with that of the aminopeptidase from Aeromonas proteolytica

The structure of PTH also resembles the three-dimensional structure of an aminopeptidase from *Aeromonas proteolytica* (Chevrier *et al.*, 1994). This peptidase contains 291 residues and two catalytic zinc ions. Although the topology of the aminopeptidase (Figure 1B) differs from that of PTH, the two three-dimensional structures and, in particular, the central twisted β-sheet, are partly superimposable. The best fit was obtained by partial alignment of the seven β-strands and of helices α1, α2, α3 and α5 of PTH, with the central core of the aminopeptidase. This core is made of seven out of the eight strands (excluding β7) of the peptidase, plus helices α4, α5, α7 and α8 (Figure 1B). The superimposition led to a final r.m.s. deviation of 2.3 Å for 102 pairs of Cα compared.

PTH behaves as an esterase. However, it is also capable of hydrolysing the amide bond between a peptide and a modified tRNA with a 3′-amino 3′-terminal adenosine (Shiloach *et al.*, 1975b). This property reinforced the validity of our comparison of the catalytic site of a peptidase with the structure of PTH. The two zinc atoms of the aminopeptidase are liganded by five residues (D117, H97, H256, E152, D179) and one water molecule (Chevrier *et al.*, 1994). H20 of PTH is superimposable on the D117 zinc ligand of the aminopeptidase (Figure 1).The side chains of D93 and H113 of PTH have approximately the same positioning as the D179 zinc ligand of the aminopeptidase, and point towards a position which in the aminopeptidase is occupied by a metal ion. Notably, the carboxylate of D93 in PTH interacts with ring nitrogens of H20 and H113. However, no strong electron density peak able to account for a metal ion could be observed in the PTH structure. Instead, well-ordered water molecules occupy the cavity of PTH. One of these water molecules is located at hydrogen bonding distances from a carboxylate oxygen of D93, from the carbonyl oxygens of L8 and H20, and from the main chain nitrogen of G23. Removal of a metal from PTH during crystallization was unlikely, because an intact and fully active enzyme was restored when the crystals were dissolved.

Nonetheless, the affinity of the enzyme for metal as well as a possible role for divalent ions in the catalytic activity of PTH were assayed by other methods. On the one hand, after dialysis of homogeneous PTH against a buffer containing 0.1 mM EDTA, zinc, cobalt, manganese and magnesium were analysed by atomic absorption spectroscopy (see Materials and methods). None of these metals could be detected with a stoichiometry greater than 0.05 mol per mol of PTH. On the other hand, the activity of PTH strongly depended on the addition of compounds such as KCl, $MgCl_2$ or spermidine (Table I), which ensure correct folding of the substrate through the shielding of its polyanionic character. In the presence of either 10 mM $MgCl_2$ or 100 mM KCl, and of di-acetyl-lysyl-$tRNA^{Lys}$ as a substrate, the catalytic activity of PTH was not modified by the addition of 100 μM of either Co^{2+}, Mn^{2+}, Zn^{2+} or Ni^{2+}, or by that of 1 mM *o*-phenanthroline.

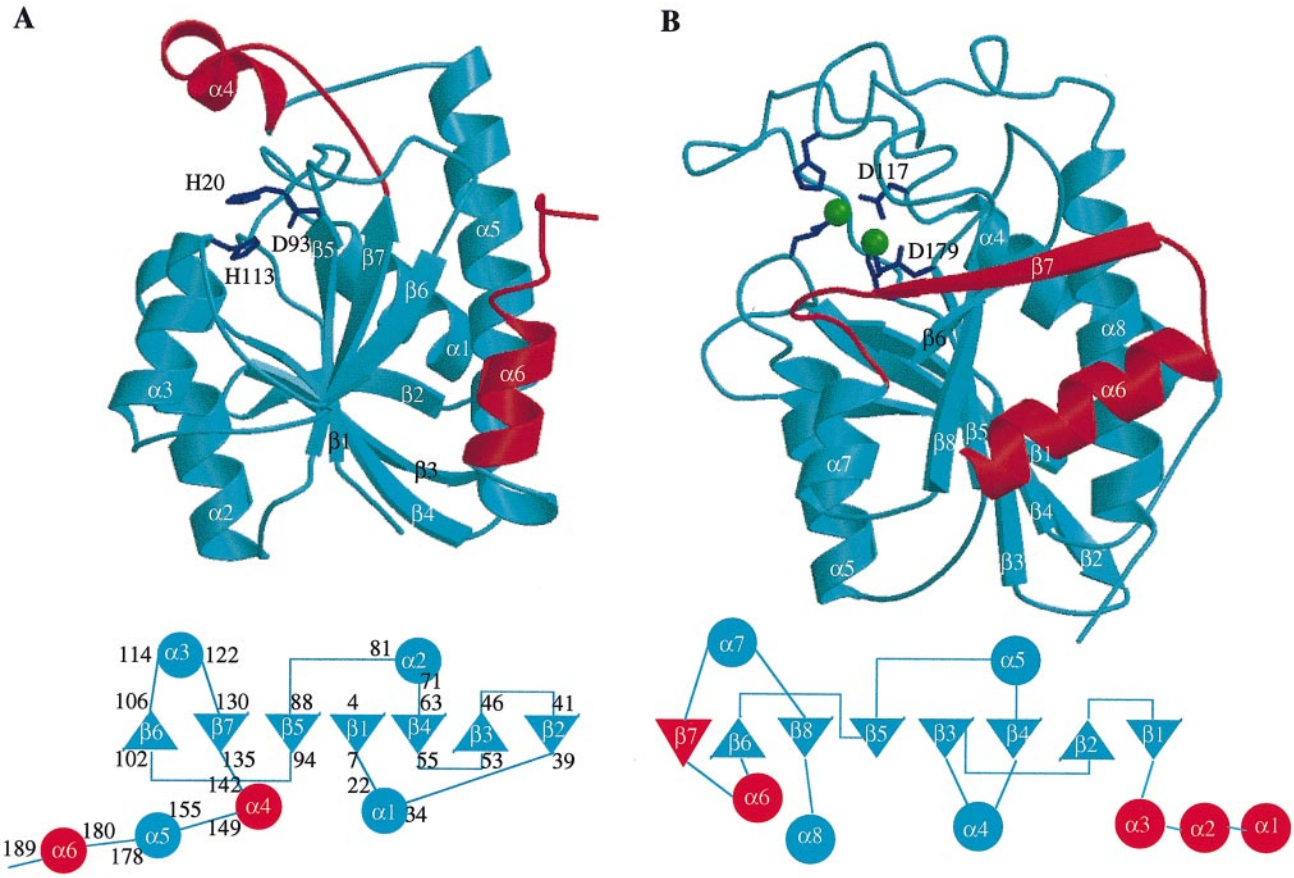

Fig. 1. Ribbon representation of peptidyl-tRNA hydrolase (PTH) from *E.coli* (**A**) and of aminopeptidase from *A.proteolytica* (**B**). Schematic representations of the enzyme topologies are shown below each structure, with the β-sheets drawn as triangles and the α-helices as circles. The ribbon representations were generated with MOLSCRIPT (Kraulis, 1991) and Raster3D (Bacon and Anderson, 1988). (A) The side chains of three residues are drawn with solid lines (see text). The two helices α4 and α6 which have no counterparts in the aminopeptidase structure are in red. Four short segments of 3_{10} helices are not represented (see Figure 2). (B) For the sake of clarity, helices α1, α2 and α3, which have no equivalent in the PTH structure, have been omitted from the ribbon drawing. Helix α6 and strand β7, which also have no counterparts in PTH, are in red. The five residues ligating the two zinc atoms drawn as green spheres, are represented with solid lines.

Table I. Activity of PTH under various assay conditions

Component added	Initial rate (s^{-1})
None	0.002
10 mM $MgCl_2$	0.4
10 mM $MgCl_2$ + 100 μM $CoCl_2$	0.4
10 mM $MgCl_2$ + 100 μM $ZnCl_2$	0.35
10 mM $MgCl_2$ + 100 μM $MnCl_2$	0.3
10 mM $MgCl_2$ + 100 μM $NiCl_2$	0.4
10 mM $MgCl_2$ + 1 mM *o*-phenantroline	0.4
100 mM KCl	0.13
100 mM KCl + 10 mM $MgCl_2$	0.13
100 mM KCl + 100 μM $CoCl_2$	0.09
100 mM KCl + 100 μM $MnCl_2$	0.05
100 mM KCl + 100 μM $NiCl_2$	0.07
1 mM spermidine-HCl	0.5

The initial rate of hydrolysis of 0.7 μM di-acetyl-[^{14}C] Lys-tRNA^{Lys} catalysed by PTH was measured as described in Materials and methods, in the presence of 20 mM Tris–HCl (pH 7.5), 0.1 mM EDTA, plus the indicated components. Measured initial rates are given within 10% accuracy.

Therefore, it appears that PTH is not and does not behave as a metalloprotein. Despite this conclusion, the resemblances between the hydrolase and the aminopeptidase enabled us to hypothesize that the cavity of PTH surrounded by residues H20, D93 and H113 corresponded to the active site. In support of the idea that histidine residues are involved in the catalysis, we obtained full inactivation of PTH upon a 10 min incubation in the presence of 1 mM diethylpyrocarbonate. In contrast, the activity of PTH was insensitive to exposure to 0.1 mM of the serine protease inhibitor phenylmethylsulfonyl fluoride (PMSF). Additional evidence in favour of the above crevice being at the catalytic centre came from alignment of the sequences of 10 known or putative PTHs. Sixteen strictly conserved residues and 28 conservative replacements were found (Figure 2). In the three-dimensional structure of *E.coli* PTH, all the strictly conserved amino acids, except the glycines, are located around the crevice delimited by the C-terminal parts of β1 and β5 and the N-terminal parts of α1 and α3 (Figure 3). Site-directed mutagenesis experiments were therefore undertaken to confirm the role of putative active site residues.

Inactivation of the pth gene on the E.coli chromosome

To produce mutated PTH species devoid of wild-type PTH of chromosomal origin, an *E.coli* strain with a disrupted *pth* gene was necessary. Application of the strategy of Hamilton *et al.* (1989) (see Materials and

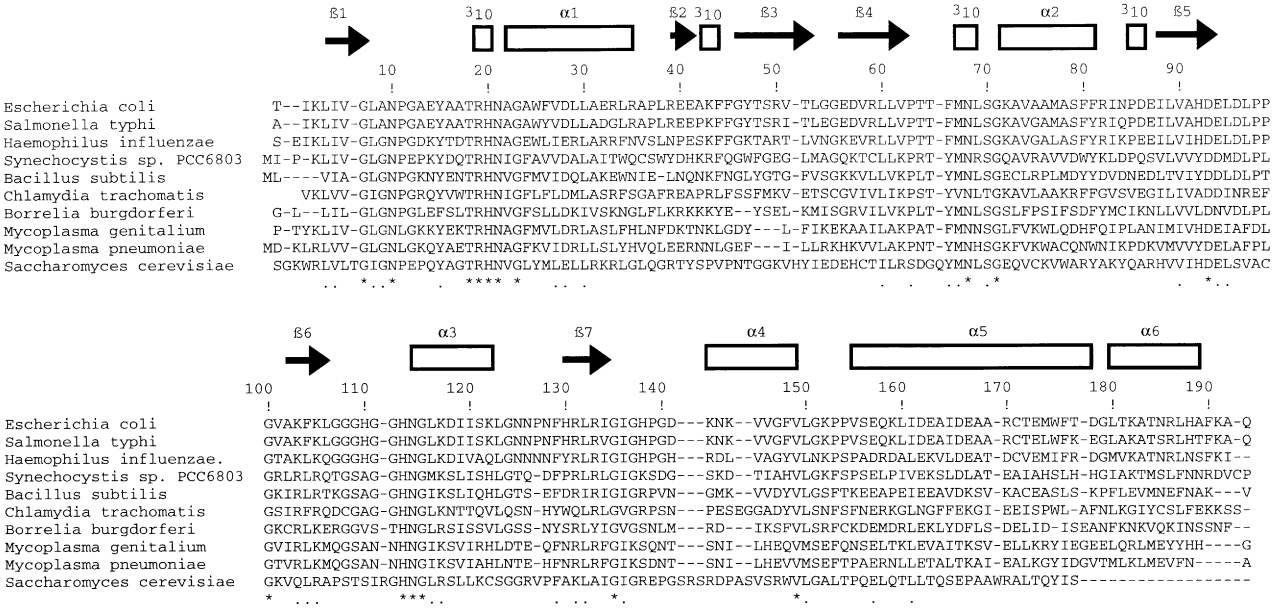

Fig. 2. Multiple sequence alignment of PTH polypeptides from various sources. The positions strictly conserved in all sequences are marked with an asterisk below the sequence. Positions with conservative replacements are signalled by a dot. The secondary structure elements of the *E.coli* protein are schematized above the sequence, with β-strands represented as arrows and helices as rods. Four short stretches of 3_{10} helices, not numbered, are indicated. The alignment was performed with the CLUSTAL V program (Higgins and Sharp, 1989).

methods) yielded a strain, K37ΔpthTr, with a disrupted copy of *pth* on the chromosome, but retaining a wild-type copy of *pth* on pMAKpth, a plasmid bearing a thermosensitive replicon derived from the pMAK705 vector. At 30°C, a permissive temperature for pMAKpth replication, K37ΔpthTr grew, albeit at a rate slightly slower than that of the *pth*$^+$ strain from which it was derived. This difference might result from a positive polar effect of *pth* on the expression of the *gpt* gene, which is immediately adjacent to *pth* on the chromosome. At the non-permissive temperature of 42°C, K37ΔpthTr no longer grew, thereby definitely establishing the essential character of *pth*. In agreement with this conclusion, the pMAKpth plasmid could be chased at 42°C provided that K37ΔpthTr had been transformed previously with pUCpth, a plasmid overexpressing wild-type PTH.

Characterization of residues crucial for the peptidyl-tRNA hydrolase activity

Site-directed mutagenesis was used to probe the role of H20, D93 and H113, as well as that of N10 and M67 which border the crevice of PTH. Because of its constrained geometry, with Ramachandran angles lying outside of the favourable regions, F66 was also included in this analysis. Each of these six residues was substituted with alanine, and the corresponding genes expressed from the pUC18 expression vector.

To analyse the activities of the mutant proteins *in vivo*, the plasmids were expressed in the context of the K37ΔpthTr strain. With the exception of the H20A mutant, overexpression of all PTH mutants enabled the chase of the pMAKpth plasmid and restored cell growth at 42°C. Such behaviour demonstrates that each of the N10A, F66A, M67A, D93A and H113A mutated proteins complement the absence of wild-type PTH.

Since after chase of the pMAKpth plasmid, the K37ΔpthTr cells contained the mutated enzymes as the only source of PTH, these enzymes could be purified free of wild-type PTH. SDS–PAGE analysis of crude extracts of K37ΔpthTr cells harbouring the pUCpth variants showed that all mutated enzymes were overexpressed. In the case of the H20A mutant, which did not support cell viability at a temperature non-permissive for pMAKpth replication, overexpression was obtained in a *pth*$^+$ context. Consequently, the H20A variant purified from pUCpthH20A in strain JM101Tr was contaminated with wild-type PTH.

The catalytic parameters of the PTH variants in the hydrolysis of di-acetyl-Lys-tRNA^{Lys} were compared with those of the wild-type enzyme (Table II). The N10A and D93A mutations reduced the catalytic efficiency by factors >100, mainly because of decreases in the k_{cat} constants. The K_m value of the substrate remained unchanged in the case of the N10A mutation, and was increased by a factor of 1.6 in the case of D93A. The catalytic efficiency of the H20A mutant was decreased by a factor of >130. These data strongly suggest that the N10, H20 and D93 residues are involved in catalysis, thereby validating the idea that the aforementioned crevice actually is the active site. The F66A, M67A and H113A mutations also affected the k_{cat} of PTH, although to smaller extents than the N10A, H20A and D93A ones.

Together with the analysis of the three-dimensional model, the results presented above designate residues belonging to the active centre of PTH.

Packing of the peptidyl-tRNA hydrolase molecules in the crystal indicates plausible positioning of the peptide product at the surface of the enzyme

As shown on the surface potential of PTH (Figure 4), the active centre makes part of a channel at the surface of the enzyme. In the crystalline form of PTH, this channel is partially occupied by three residues of the C-end of a neighbouring protein molecule. These residues establish

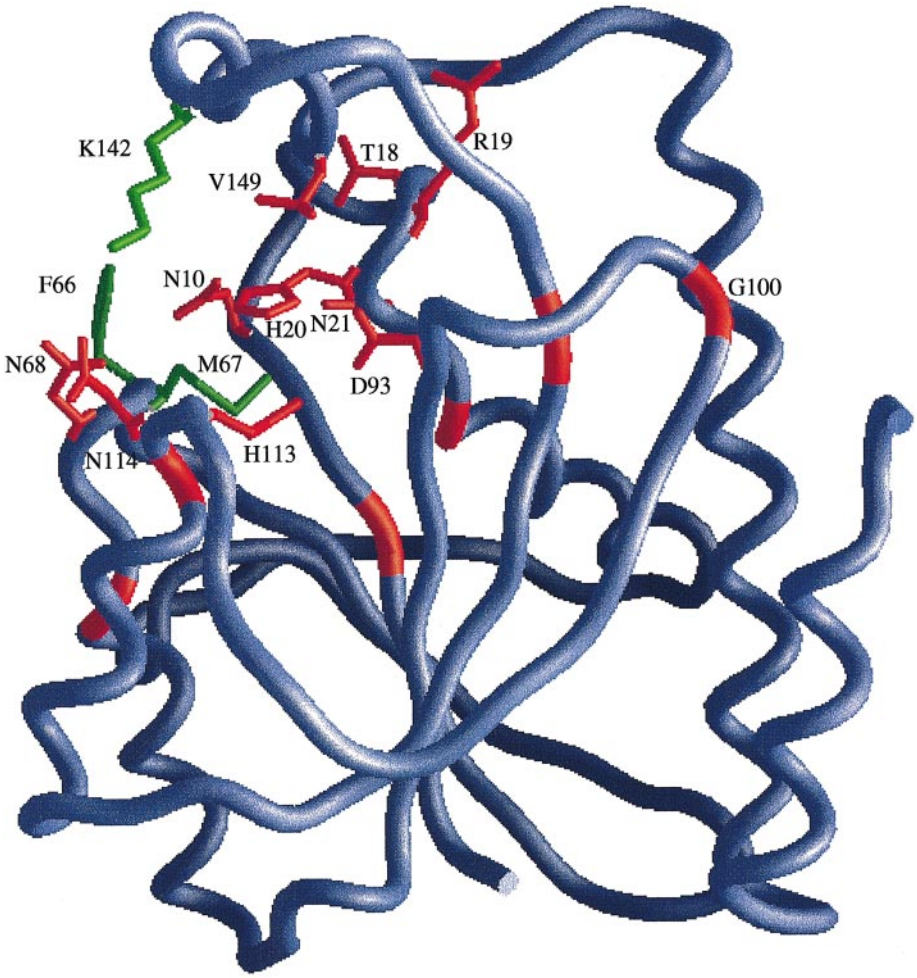

Fig. 3. Location of the conserved residues (see Figure 2) in the three-dimensional model of *E.coli* PTH. The Cα trace of the PTH molecule is drawn. The positions of the conserved Gly residues are indicated as red segments. Residue Gly100, whose mutation into Asp is responsible for thermosensitive *E.coli* growth (Garcia-Villegas *et al.*, 1991), is labelled. The side chains of the non-glycine residues conserved in the PTH sequences are drawn as red sticks and labelled. Three non-conserved residues (F66, M67 and K142), included in our site-directed mutagenesis study, are shown in green. The figure was generated with Grasp (Nicholls *et al.*, 1991).

Table II. Catalytic parameters of the PTH variants

Enzyme	k_{cat} (s^{-1})	K_m (μM)	k_{cat}/K_m (relative)
WT	3.6 ± 0.2	6.0 ± 0.7	100
N10A	0.028 ± 0.002	6.6 ± 1.0	0.8
H20A	n.m.	n.m.	<0.8[a]
M67A	0.17 ± 0.02	4.1 ± 0.6	6.7
F66A	0.9 ± 0.1	6.9 ± 0.9	33
D93A	0.05 ± 0.01	10 ± 2	0.8
H113A	1.2 ± 0.2	8.8 ± 2.8	23
K142A	>1.8	>30	10
WT[b]	0.85 ± 0.11	24 ± 4	5.8
K142A[b]	n.d.	n.d.	0.8

The inital rates of hydrolysis of di-acetyl-lysyl-$tRNA^{Lys}$ (from 0.7 to 25 μM) were measured as described in Materials and methods.
[a]The H20A enzyme preparation is contaminated by wild-type PTH. Consequently, the catalytic efficiency measured with this sample (0.8%) must be greater than that of the H20A mutant enzyme.
[b]Parameters measured with 5′-dephosphorylated di-acetyl-lysyl-$tRNA^{Lys}$ as substrate.
n.m., not measurable; n.d., not determined.

close electrostatic contacts with several residues belonging to the active centre. As a consequence, the C-terminal residues of PTH are well ordered in the crystal, although they protrude outside of the protein. One possibility is that the C-end of a PTH molecule bound to another one mimics the peptide product in the catalytic site. Because of the physiological role of PTH, specificity towards the sequence of the peptidic moiety of a peptidyl-tRNA substrate is expected to be broad. Accordingly, the contacts between the C-end of PTH ($_{191}KAQ_{193}$) and the active site crevice only involve main chain atoms of the former. More precisely, electrostatic bonds occur between the terminal oxygens of Q193 and the amide nitrogens of N114 and N68, between the main chain oxygen of A192 and the amide nitogen of N10, and between the main chain oxygen of K191 and the main chain nitrogen of N68. Finally, an additional hydrogen bond occurs between the main chain oxygen of H188 and the hydroxyl of Y15. Such a network clearly indicates that the aforementioned channel at the surface of PTH can accommodate the carbonyl groups and the free carboxylate of any tripeptide. Interestingly, N68 and N114, which are involved in this binding, are strictly conserved in all the PTH sequences of Figure 2.

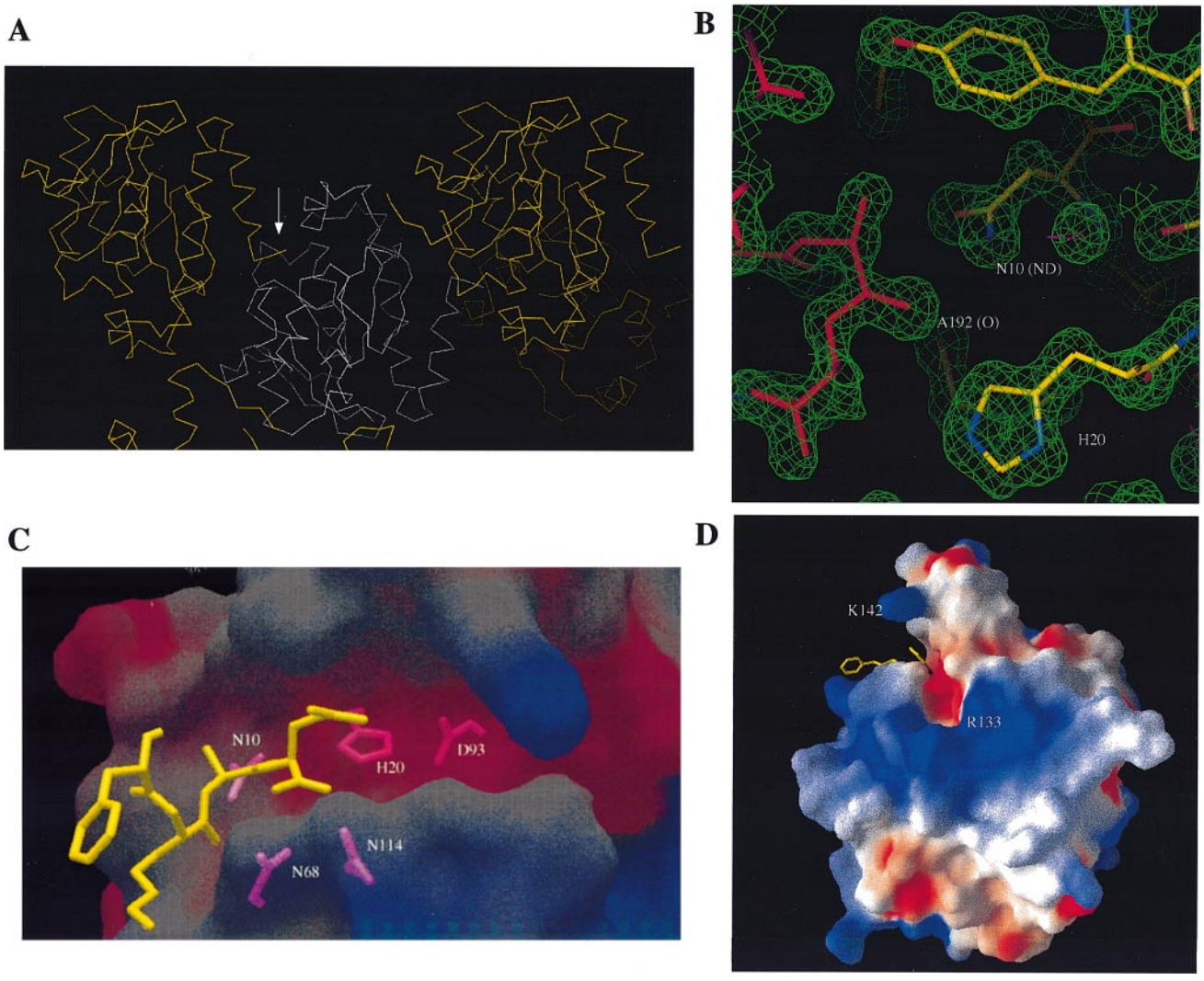

Fig. 4. (**A**) Schematic representation of the packing of PTH molecules in the crystal. The Cα traces of PTH molecules are represented, with a reference molecule shown in white and neighbouring molecules in yellow. The arrow indicates the C end of a PTH molecule packed within the active centre of the reference molecule. For the sake of clarity, only some of the neighbours are represented. (**B**) View of the 1.2 Å resolution $2F_o–F_c$ map contoured at 1.8 standard deviation above its mean value, showing the contact between the amide nitrogen of N10 (N10, ND) and the carbonyl oxygen of the last peptidic bond at the C end of a neighbouring PTH molecule (A192, O). The side chains of H20 and Y15 are visible. Note that rotation of the imidazole ring of H20 by 180° would provide a hydrogen bond between the δN and the carbonyl oxygen of A192. However, such a rotation would break a tight hydrogen bond of this δN with the carboxylate of D93. The purple triangle represents a water molecule. (A) and (B) were drawn using the program O (Jones *et al.*, 1991). (**C**) Close view of the active site channel, with the four C-terminal residues of a neighbouring enzyme molecule shown as yellow sticks. The representation is the same as that of (D), except that the surface was made transparent in order to view the side chains of enzyme residues shown in purple. Represented are N10, N68 and N114, involved in the binding of main chain atoms of the three C-terminal residues of the neighbouring molecule, as well as H20 and D93, shown in this study to be crucial for enzyme activity. (**D**) Molecular surface of the protein showing the electrostatic potential calculated with the Delphi program (Nicholls and Honig, 1991) and rendered with Grasp (Nicholls *et al.*, 1991). Negatively charged regions are coloured in red and positively charged areas are in blue. The four C-terminal residues of a neighbouring PTH molecule, drawn as solid sticks, are visible at the back of the figure. The position of R133, whose mutation into His is responsible for the Rap phenotype (Garcia-Villegas *et al.*, 1991), is indicated, as well as that of K142.

Binding of the tRNA moiety of the substrate by peptidyl-tRNA hydrolase

The surface potential of PTH highlighted two cationic regions possibly involved in the binding of the tRNA moiety of the substrate (Figure 4). The first one borders the active site and is located at the opposite side of the part of the channel occupied in the crystal by the C-terminus of a neighbouring protein molecule. An involvement of this region in the activity of PTH is indicated by the sensitivity of R133 to mutation. Indeed, an *E.coli* strain with a *pth* gene carrying the R133H mutation shows PTH activity reduced by a factor of 10 (Henderson and Weil, 1976; Garcia-Villegas *et al.*, 1991).

The second region corresponds to the α4 helix making a lid over the active site crevice. This helix is surrounded by glycine residues (G135, G140 and G151), indicative of mobility. Accordingly, the average temperature factors of the helix residues are among the highest in the three-dimensional structure. K142 of the helix points towards the catalytic crevice and might interact with tRNA. To investigate this idea, a K142A variant, capable upon overexpression of supporting the growth of the K37ΔpthTr strain at 42°C, was purified to homogeneity. Catalytic parameters of this enzyme are compared with those of wild-type PTH in Table II. The K_m value for the hydrolysis of di-acetyl-Lys-tRNA^{Lys} was increased by a factor of >5,

and could not be determined accurately. In contrast, the k_{cat} value was not reduced by a factor >2. These results are in agreement with the participation of K142 in the productive binding of the tRNA moiety. One possibility was that this lysine recognized the 5′ phosphate group of tRNA. However, as shown in Table II, the 5′ dephosphorylation of di-acetyl-Lys-tRNA^{Lys} had similar relative consequences on the activity of either the wild-type enzyme or the K142A mutant. This result tends to exclude an interaction of the K142 side chain with the 5′ phosphate group of the tRNA.

Concluding remarks

PTH is a single domain enzyme built around a twisted mixed β-sheet. It shares some three-dimensional structure similarities with the zinc-dependent aminopeptidase from *A.proteolytica* (Chevrier *et al.*, 1994). However, the mechanisms of action of these two enzymes appear different. In particular, a role for a metal ion could not be evidenced in the reaction sustained by the hydrolase. Despite the different topologies of the two enzymes, their comparison was helpful in the identification of residues important for PTH activity. Three residues, N10, H20 and D93, appear deeply involved in the enzyme action. The counterparts of two of these residues in the three-dimensional architecture of the peptidase are at the catalytic centre, where they strongly bind two zinc ions. In the hydrolase crystal structure, the pocket corresponding to the above residues is occupied by the C-end of a neighbouring PTH molecule. One of the packing contacts responsible for this interaction involves the N10 residue on the one hand, and the main chain carbonyl of the last peptidic bond (192–193) of PTH on the other hand. We assume that the binding of the last three residues of one PTH molecule to another PTH molecule corresponds to a product complex of the hydrolase. Interestingly, according to this hypothesis, N10 would interact with that amide bond of the substrate which is absolutely required for enzyme action. Indeed, this amide bond corresponds to the N-blocked moiety which an aminoacyl-tRNA has to carry in order to be a substrate. To be an optimal substrate of PTH, a peptidyl-tRNA must carry at least four amino acid residues (Shiloach *et al.*, 1975a). Notably, three residues of one PTH molecule occupy the active site of another PTH molecule in the crystal. Consequently, the binding of three residues of one PTH molecule in the active site of another PTH molecule may also resemble that of a tri-peptide esterified to tRNA. In this case, the site of cleavage of the ester bond would be close to N68, N114 and H20, all three of which are strictly conserved in the available PTH sequences. In this model, the ester bond would be presented in a productive manner to the active centre through tRNA interaction with the positively charged protein area typified by the R133 residue. Since the distance between R133 and N68 is relatively short (~19 Å) with respect to the size of a tRNA, the elements of tRNA recognized by PTH should be concentrated in a small region, possibly in the acceptor stem. Further studies are required to validate the above ideas and to assess possible conformational changes (Shiloach *et al.*, 1975a) upon complex formation.

Materials and methods

Crystallization and data collection

PTH was purified from overproducing cells as described (Dutka *et al.*, 1993; Schmitt *et al.*, 1997). Suitable crystals for X-ray experimentation were obtained by using polyethylene glycol as precipitant and isopropanol as additive (Schmitt *et al.*, 1997). Crystals obtained using these conditions were orthorhombic, space group $P2_12_12_1$, with unit cell dimensions a = 47.2 Å, b = 63.6 Å and c = 62.6 Å. For data collection and soaking, crystals were stabilized in 14% (v/v) polyethylene glycol, 12% (v/v) isopropanol, 0.1 mM Tris–HCl pH 7.5. Mercury derivatives were prepared by soaking native crystals in 5 mM PCMBS, or in 5 mM PHMB, for 5 days. Lead derivatives were obtained by soaking native crystals in 30 mM TMLA for 5 days. Platinate crystals were obtained by soaking native crystals in 2.5 mM $KPtCl_4$ for 5 days (Table III). Data were collected at 0°C by using the Synchrotron (λ = 0.994 Å) at L.U.R.E (Orsay, France) on a MAR-Research phosphor image plate system (Hamburg, Germany), or on a rotating anode source (Siemens, Karlsruhe, Germany) with a Hi-star area detector (Siemens, Karlsruhe, Germany). Diffraction images were analysed either with the MOSFLM program (A.G.W.Leslie, Laboratory of Molecular Biology, Daresbury, UK) or with the XDS program (Kabsch, 1988), and the data was processed further using programs from the CCP4 package (Collaborative Computational Project No. 4, 1994).

Heavy atom and phase determination

For each atom derivative, sites were localized using difference Patterson syntheses. The position of the strongest site of the mercury atom of the PCMBS derivative was first identified. Further, this major site and the CCP4 program MLPHARE (Otwinowski, 1991) were used to calculate SIR (single isomorphous replacement) phases, which were then used to compute difference Fourier maps. From these maps, the position of the minor site of the mercury atom of the PCMBS derivative as well as the positions of the heavy atoms in the other derivatives were determined iteratively. For all new sites, the Patterson maps were checked systematically with the help of the PATGEN program (Chevrier, 1994). The combination of all derivatives allowed the determination of MIR phases by using the MLPHARE program. The mean figures of merit in the resolution range of 12–3.0 Å were 0.79 for the centric data and 0.65 for the acentric data (Table III).

Model building

The determination of MIR phases allowed the calculation of MIR maps at 3.5 and 3.0 Å resolution. The phases were then improved by solvent flattening and histogram matching using the DM program (Cowtan, 1994). In the resulting density maps, the secondary structures could be clearly identified, and model building was undertaken with the aid of bones [calculated using MAPMAN (Kleijwegt and Jones, 1994)] and the O program (Jones *et al.*, 1991). The quality of the maps was such that all the peptidic backbone of the molecule could be constructed. The amino acid sequence was then aligned with the electron density by indentifying some well-defined aromatic residues. In particular the sequence $_{44}$FFGY$_{47}$ of the PTH was used as the starting point for the sequence assignment. Hence, the complete amino acid sequence including residues 1–193 could be fitted unambiguously in the electron density.

Refinement

The model was first refined against the 8.0–3.5 Å native data (2σ cut-off) using the program X-PLOR (Brünger, 1992a). The crystallographic *R*-factor for the starting model was 42.3%. A random sample containing 6% of the total data (3276 out of 53 921 reflections) was excluded from the refinement and the agreement between calculated and observed structure factors for these reflections (*R*-free) was used to monitor the course of the refinement procedure (Brünger, 1992b). A round of positional refinement and simulated annealing (Brünger *et al.*, 1987) was performed by increasing the resolution to 2.35 Å. In parallel, the *R*-factor was lowered to 0.280 and *R*-free to 0.332. Refinement of the atomic positions and of temperature factors was carried out. In this way, resolution was gradually increased to 1.2 Å. Positive peaks in F_o–F_c maps were assigned as water molecules provided they had heights greater than four standard deviations above the mean value, and were at acceptable distances from protein and solvent polar atoms. A total of 181 water molecules were added. Finally, alternative conformations were refined for 11 side chains. In each case, these alternative conformations did not differ much from one another. The final *R*-factor of the refined model was 19.6% for all reflections between 8.0 and 1.2 Å (2σ cut-off).

Table III. Native and heavy atom derivative data used in structure determination of peptidyl-tRNA hydrolase

Data set	Native	PCMBS	PHMB	$KPtCl_4$	TMLA
Reagent concentration (mM)		5	2.5	2.5	30
Soaking time (days)		5	5	7	2
X-ray source	LURE W32	Lab.	Lab.	Lab.	Lab.
Processing	MOSFLM	XDS	XDS	XDS	XDS
Resolution (Å)	30–1.2	12–3.0	12–3.0	12–3.0	12–3.0
Completeness	93.9 (85.3)	87.6 (82.6)	61.4 (56.7)	84.9 (76.0)	86.0 (82.9)
Redundancy	4.2	2.2	3.1	2.2	2.4
R_{sym} (I) (%)[a]	4.6 (15)	3.7 (4.4)	4.1 (4.9)	4.7 (6.4)	3.4 (4.3)
ΔF_{iso} (%)[b]		28.2	25.6	23.2	12.6
No. of heavy atom sites		2	1	6	2
R_{Cullis}[c]		0.5	0.56	0.76	0.77
Phasing power[d]					
centric		1.81	1.56	0.78	0.72
acentric		2.32	1.92	1.12	1.05
Mean overall figure of merit	0.62 at 3.0 Å				

Each data set was collected with a single crystal. The values in parentheses correspond to the highest shell of resolution. The derivatives are: PCMBS, sodium parachloromercuriphenylsulfonate; PHMB, sodium parahydroxymercuribenzoate; $KPtCl_4$, potassium tetrachloroplatinate: TMLA, trimethyllead acetate.

[a] $R_{sym}(I) = \sum_{hkl}\sum_{i}|\langle I_{hkl}\rangle - I_{hkl,i}|/\sum_{hkl}\sum_{i}|I_{hkl}|$ where i is the number of reflection hkl.

[b] $\Delta F_{iso} = \sum_{hkl}|Fph_{hkl} - Fp_{hkl}|/\sum_{hkl} Fp_{hkl}$ where Fph are the structure factors of the derivative and Fp those of the native crystal.

[c] $R_{Cullis} = \sum_{hkl}|Fph - |\vec{Fp} + \vec{Fh}||/\sum_{hkl}|Fph - Fp|$ for the centric terms only. Fh are the structure factors of the heavy atom.

[d] Phasing power $= [\sum_{hkl}|Fh|^2/\sum_{hkl}(|Fph|^2 - |Fph(calc)|^2]^{1/2}$.

R-free was 21.5%. The stereochemistry and geometry were analysed using the program PROCHECK (Laskowski *et al.*, 1993). Co-ordinates have been deposited to the Brookhaven Protein Data Bank (accession No. 2pth) where they will be held for 1 year.

Site-directed mutagenesis

The *pth* gene was cloned into the M13mp19 phage vector by inserting the *Eco*RI–*Hin*dIII fragment from pUCpth. Oligonucleotide site-directed mutagenesis was then performed by using the resulting M13PTH single-stranded DNA as template, as previously described (Sayers *et al.*, 1988). The mutated genes were sequenced completely prior to re-insertion into the pUC18 expression vector. With mutant PTH capable of complementing the Δ*pth* mutation of K37ΔpthTr (see below), the corresponding enzymes were produced in this strain in order to exclude contamination by wild-type PTH. This strategy applied to all mutants studied, except H20A which had to be produced in a pth^+ context (strain JM101Tr; Hirel *et al.*, 1988).

Inactivation of the pth gene and purification of PTH variants

Disruption of the *pth* gene was achieved by the method of Hamilton *et al.* (1989). The *pth* gene in pUCpth (Dutka *et al.*, 1993) was subcloned into pMAK705, a plasmid with a thermosensitive replicon carrying a chloramphenicol resistance gene (Hamilton *et al.*, 1989). The 94 bp *Msc*I fragment of the *pth* gene was replaced by the Kan^r cassette from pUC4K (Pharmacia, Uppsala, Sweden), to give pMAKpthΔK. This plasmid was used to transform the *E.coli* strain K37 (*galK*, *rpsL*). The integration of pMAKpthΔK into the chromosome was selected by plating transformants at 42°C on LB-agar medium containing chloramphenicol. After subsequent growth at 30°C for ~40 generations, cells no longer carrying the plasmid in their chromosome were identified as chloramphenicol-sensitive colonies at 42°C. Approximately 40% of the selected clones also displayed thermosensitivity in the absence of chloramphenicol, thus showing that the only functional *pth* gene was carried by the plasmid and that the chromosomal *pth* gene had been replaced by the inactivated copy. One of these latter clones was made recombination deficient by transducing the *recA56* allele from the Hfr strain JC10240 (Csonka and Clark, 1980), to give K37ΔpthTr. This strain contains a disrupted *pth* gene on its chromosome, and an active copy of *pth* on the thermosensitive pMAKpth plasmid.

K37ΔpthTr cells were transformed at 30°C by a pUCpth plasmid containing the *pth* gene with the desired mutation. Transformed cells were then plated at 42°C on LB medium containing ampicillin to chase pMAKpth, and purified twice at 37°C. The chase of the plasmid was verified by ensuring that the cells obtained had become chloramphenicol sensitive at 30°C. Cells in 1 l cultures were grown overnight in 2× TY medium containing 50 μg/ml ampicillin and 0.3 mM isopropyl-β-D-thiogalactopyranoside (IPTG). Preparation of crude extracts and chromatography on Q-Sepharose and SP-Sepharose were performed as described previously (Schmitt *et al.*, 1997). According to SDS–PAGE analysis, purified PTH variants were at least 95% homogeneous.

Preparation of di-acetyl-lysyl-tRNA^{Lys}

Escherichia coli $tRNA^{Lys}$ was overexpressed in strain JM101TR from a synthetic gene built as described previously (Commans *et al.*, 1995). Crude tRNA extract from this strain accepted 800 pmol of lysine per A_{260} unit. $tRNA^{Lys}$ in this extract was fully lysylated within 5 min at 28°C in 4 ml of 20 mM Tris–HCl (pH 7.5), 7 mM $MgCl_2$, 0.1 mM EDTA, 60 μM [^{14}C]L-lysine (50 Ci/mol), 2 mM ATP, 120 μM tRNA and 2 μM *E.coli* LysS lysyl-tRNA synthetase (Brevet *et al.*, 1995). The reaction was quenched by the addition of 450 μl of 3 M sodium acetate (pH 5.5) and precipitation with ethanol. The tRNA pellet was dissolved in 0.8 ml of 5 mM sodium acetate (pH 5.5) and centrifuged. Acetylation of the supernatant was achieved at 0°C for 45 min by adding 1 ml of dimethylsulfoxide, 0.2 ml of glacial acetic acid and 0.2 ml of acetic anhydride. After ethanol precipitation and centrifugation, the pellet was dissolved in 0.5 ml of a solution containing 10 mM $CuSO_4$ and 0.36 M sodium acetate (pH 5.5), as described (Dutka *et al.*, 1993). After 30 min at 37°C, the sample was precipitated with ethanol and centrifuged. To remove remaining copper ions, the tRNA pellet was dissolved in 400 μl of a 20 mM sodium acetate buffer (pH 5.5) containing 100 mM KCl (buffer A), and chromatographed on a Chelex 100 column (200 μl) equilibrated in buffer A. Finally, the di-acetyl-lysyl-$tRNA^{Lys}$ was precipitated in ethanol and stored at –20°C. Before use, it was centrifuged and the pellet was redissolved in 5 mM sodium acetate (pH 5.5) containing 0.1 mM EDTA.

Dephosphorylation of tRNA^{Lys}

Dephosphorylation of 500 pmol of tRNA was carried out in 50 μl of 50 mM Tris–HCl (pH 8.5), 0.1 mM EDTA and 2.5 U of alkaline phosphatase from calf intestine (Pharmacia) for 30 min at 55°C. Rephosphorylation in 20 μl was performed at 37°C for 30 min in 50 mM Tris–HCl (pH 8), 10 mM $MgCl_2$ containing 25 μM [γ-^{33}P]ATP

(50 Ci/mmol) and 20 U of polynucleotide kinase (Pharmacia). The resulting labelled tRNA was used subsequently as a probe to follow large-scale dephosphorylation of $tRNA^{Lys}$. A 500 µl mixture containing 20 mM Tris–HCl (pH 8.5), 0.1 mM EDTA, 500 pmol of ^{33}P-labelled tRNA, 150 nmol of unlabelled tRNA and 12.5 U of alkaline phosphatase was incubated at 55°C. After 60 min, an aliquot was withdrawn and precipitated with 5% trichloracetic acid (TCA), filtered and counted. Less than 0.1% of the initial radioactivity had remained bound to tRNA. The remaining part of the sample was precipitated with ethanol, aminoacylated and acetylated as described above.

Peptidyl-tRNA hydrolase assay

Peptidyl-tRNA hydrolase activity was measured at 28°C in 100 µl assays containing 20 mM Tris–HCl (pH 7.5), 10 mM $MgCl_2$, 0.1 mM EDTA, 0.7–25 µM di-acetyl-[^{14}C]Lys-$tRNA^{Lys}$ and catalytic amounts of PTH. The reaction was quenched by the addition of 100 µl of 5% TCA and 20 µl of carrier RNA from yeast (4 mg/ml). The sample was centrifuged and the released di-acetyl-[^{14}C]lysine was measured in the supernatant by scintillation counting, as described (Dutka *et al.*, 1993). K_m and k_{cat} values were derived from iterative non-linear fits of the theroretical Michaelis equation to the experimental values, using the Levenberg–Marquardt algorithm. Confidence limits on the fitted values were obtained by 100 Monte-Carlo simulations followed by least-squares fitting, using the experimental standard deviations on individual measurements (Dardel, 1994).

Atomic absorption spectroscopy

Metal atomic absorbancies were measured at appropriate wavelengths in the peak height mode during 5 s after 0.1 ml injections, using a Varian AA775 spectrophotometer equipped with an air–acetylene burner (Mayaux and Blanquet, 1981; Fourmy *et al.*, 1993). Prior to metal analysis, PTH was dialysed extensively against a buffer containing 20 mM Tris–HCl pH 7.5, 10 mM 2-mercaptoethanol, 100 mM KCl and 0.1 mM EDTA. Standard solutions containing various metal concentrations (5–50 µM) were prepared by dilution in the same buffer.

Acknowledgements

We are much indebted to Dino Moras and all his colleagues at the 'Unité de Biologie structurale' (UPR CNRS No. 9004, Illkirch, France), and in particular to Jean Cavarelli, André Mitschler, Marc Ruff and Jean-Claude Thierry, for their kind hospitality during data collection. Roger Fourme and Marc Schiltz (Laboratoire pour l'Utilisation du Rayonnement Electromagnétique, UMR CNRS No. 130 Orsay, France) are gratefully acknowledged for assistance during data collection at the beamline DW32.

References

Atherly,A.G. (1978) Peptidyl-transfer RNA hydrolase prevents inhibition of protein synthesis initiation. *Nature*, **275**, 769.

Atherly,A.G. and Menninger,J.R. (1972) Mutant *E.coli* strain with temperature sensitive peptidyl-transfer RNA hydrolase. *Nature New Biol.*, **240**, 245–246.

Bacon,D.J. and Anderson,W.F. (1988) A fast algorithm for rendering space-filling molecule pictures. *J. Mol. Graph.*, **6**, 219–220.

Brevet,A., Chen,J., Lévêque,F., Blanquet,S. and Plateau,P. (1995) Comparison of the enzymatic properties of the two *Escherichia coli* lysyl-tRNA synthetase species. *J. Biol. Chem.*, **270**, 14439–14444.

Brünger,A.T. (1992a) *X-PLOR Version 3.1. A System for X-ray Crystallography and NMR*. Yale University Press, New Haven, CT.

Brünger,A.T. (1992b) Free-*R* value: a novel statistical quantity for assessing the accuracy of crystal structures. *Nature*, **355**, 472–474.

Brünger,A.T., Kuryian,J. and Karplus,M. (1987) Crystallographic *R*-factor refinement by molecular dynamics. *Science*, **235**, 458–460.

Chapeville,F., Yot,P. and Paulin,D. (1969) Enzymatic hydrolysis of *N*-acylaminoacyl transfer RNAs. *Cold Spring Harbor Symp. Quant. Biol.*, **34**, 493–498.

Chevrier,B. (1994) PATGEN: an automatic program to generate theoretical Patterson peaks and to compare them with experimental Patterson peaks. *J. Appl. Crystallogr.*, **27**, 860–861.

Chevrier,B., Schalk,C., D'Orchymont,H., Rondeau,J.M., Moras,D. and Tarnus,C. (1994) Crystal structure of *Aeromonas proteolytica* aminopeptidase: a prototypical member of the co-catalytic zinc enzyme family. *Structure*, **2**, 283–291.

Collaborative Computational Project No. 4 (1994) The CCP4 suite: programs from protein crystallography. *Acta Crystallogr.*, **D50**, 760–763.

Commans,S., Plateau,P., Blanquet,S. and Dardel,F. (1995) Solution structure of the anticodon binding domain of *Escherichia coli* lysyl-tRNA synthetase and studies of its interaction with $tRNA^{Lys}$. *J. Mol. Biol.*, **253**, 100–113.

Cowtan,K. (1994) dm: an automated procedure for phase improvement by density modification. *Joint CCP4 and ESF-EACBM Newsletter on Protein Crystollagraphy*, **31**, 34–38.

Csonka,L.N. and Clark,A.J. (1980) Construction of an Hfr strain useful for transferring *recA* mutations between *Escherichia coli* strains. *J. Bacteriol.*, **143**, 529–530.

Cuzin,F., Kretchmer,N., Greenberg,R.E., Hurwitz,R. and Chapeville,F. (1967) Enzymatic hydrolysis of *N*-substituted aminoacyl-tRNA. *Proc. Natl Acad. Sci. USA*, **58**, 2079–2086.

Dardel,F. (1994) MC-Fit: Using Monte-Carlo methods to get accurate confidence limits on enzyme parameters. *CABIOS*, **10**, 273–275.

Dutka,S., Meinnel,T., Lazennec,C., Mechulam,Y. and Blanquet,S. (1993) Role of the 1–72 base pair in tRNAs for the activity of *Escherichia coli* peptidyl-tRNA hydrolase. *Nucleic Acids Res.*, **21**, 4025–4030.

Fourmy,D., Meinnel,T., Mechulam,Y. and Blanquet,S. (1993) Mapping of the zinc binding domain of *Escherichia coli* methionyl-tRNA synthetase. *J. Mol. Biol.*, **231**, 1068–1077.

Garcia-Villegas,M.R., De La Vega,F.M., Galindo,J.M., Segura,M., Buckingham,R.H. and Guarneros,G. (1991) Peptidyl-tRNA hydrolase is involved in λ inhibition of host protein synthesis. *EMBO J.*, **10**, 3549–3555.

Gross,M., Crow,P. and White,J. (1992a) The site of hydrolysis by rabbit reticulocyte peptidyl-tRNA hydrolase is the 3′-AMP terminus of susceptible tRNA substrates. *J. Biol. Chem.*, **267**, 2080–2086.

Gross,M., Starn,T.K., Rundquist,C., Crow,P., White,J., Olin,A. and Wagner,T. (1992b) Purification and initial characterization of peptidyl-tRNA hydrolase from rabbit reticulocytes. *J. Biol. Chem.*, **267**, 2073–2079.

Guillon,J.M., Meinnel,T., Mechulam,Y., Lazennec,C., Blanquet,S. and Fayat,S. (1992) Nucleotides of tRNA governing the specificity of *Escherichia coli* methionyl-$tRNA^{Met}_f$ formyltransferase. *J. Mol. Biol.*, **224**, 359–367.

Hamilton,C.M., Aldea,M., Washburn,B.K., Babitzke,P. and Kushner,S.R. (1989) New method for generating deletions and gene replacements in *Escherichia coli*. *J. Bacteriol.*, **171**, 4617–4622.

Henderson,D. and Weil,J. (1976) A mutant of *Escherichia coli* that prevents growth of phage lambda and is bypassed by lambda mutants in a nonessential region of the genome. *Virology*, **71**, 546–559.

Heurgue-Hamard,V., Mora,L., Guarneros,G. and Buckingham,R.H. (1996) The growth defect in *Escherichia coli* deficient in peptidyl-tRNA hydrolase is due to starvation for Lys-$tRNA^{Lys}$. *EMBO J.*, **15**, 2826–2833.

Higgins,D.G. and Sharp,P.M. (1989) Fast and sensitive multiple sequence alignments on a microcomputer. *CABIOS*, **5**, 151–153.

Hirel,P.-H., Lévêque,F., Mellot,P., Dardel,F., Panvert,M., Mechulam,Y. and Fayat,G. (1988) Genetic engineering of methionyl-tRNA synthetase: *in vitro* regeneration of an active synthetase by proteolytic cleavage of a methionyl-tRNA synthetase-β-galactosidase chimeric protein. *Biochimie*, **70**, 773–782.

Jones,T.A., Zou,J.Y., Cowan,S.W. and Kjeldgaard,M. (1991) Improved methods for the building of protein models in electron density maps and the location of errors in these models. *Acta Cystallogr.*, **A47**, 110–119.

Jost,J.P. and Bock,R.M. (1969) Enzymatic hydrolysis of *N*-substituted aminoacyl transfer ribonucleic acid in yeast. *J. Biol. Chem.*, **244**, 5866–5873.

Kabsch,W.J. (1988) Evaluation of single crystal X-ray diffraction data from a position sensitive detector. *J. Appl. Crystallogr.*, **21**, 916–924.

Kleijwegt,G.J. and Jones,T.A. (1994) *Proceedings of the CCP4 Study Weekend: From First Map to Final Model*. SERC Daresbury Laboratory, Warrington, UK, pp. 59–66.

Koellner,G., Luic,M., Shugar,D., Saenger,W. and Bzowska,A. (1997) Crystal structure of calf spleen purine nucleoside phosphorylase in a complex with hypoxanthine at 2.15 Å resolution. *J. Mol. Biol.*, **265**, 202–216.

Kössel,H. (1969) Purification and properties of peptidyl-tRNA hydrolase from *Escherichia coli*. *Biochim. Biophys. Acta*, **204**, 191–202.

Kössel,H. and RajBhandary,U.L. (1968) Studies on polynucleotides. LXXXVI. Enzymic hydrolysis of *N*-acylaminoacyl-transfer RNA. *J. Mol. Biol.*, **35**, 539–560.

Kraulis,P. (1991) A program to produce both detailed and schematic plots of protein structures. *J. Appl. Crystallogr.*, **24**, 946–950.
Laskowski,R.A., Mac Arthur,M.W., Moss,D.S. and Thornton,J.M. (1993) PROCHECK: a program to check the stereochemical quality of protein structure. *J. Appl. Crystallogr.*, **26**, 283–291.
Lee,C.P., Seong,B.L. and RajBhandary,U.L. (1991) Structural and sequence elements important for recognition of *Escherichia coli* formylmethionine tRNA by methionyl-tRNA transformylase are clustered in the acceptor stem. *J. Biol. Chem.*, **266**, 18012–18017.
Luzatti,P.V. (1952) Traitement statistique des erreurs dans la détermination des structures cristallines. *Acta Crystallogr.*, **5**, 802–810.
Mayaux,J.-F. and Blanquet,S. (1981) Binding of zinc to *Escherichia coli* phenylalanyl transfer ribonucleic acid synthetase. Comparison with other aminoacyl transfer ribonucleic acid synthetases. *Biochemistry*, **20**, 4647–4654.
Menninger,J.R. (1976) Peptidyl-transfer RNA dissociates during protein synthesis from ribosomes of *Escherichia coli*. *J. Biol. Chem.*, **251**, 3392–3398.
Menninger,J.R. (1978) The accumulation as peptidyl-transfer RNA of isoaccepting transfer RNA families in *E.coli* with temperature-sensitive peptidyl-tRNA hydrolase. *J. Biol. Chem.*, **253**, 6808–6813.
Menninger,J.R. (1979) Accumulation of peptidyl-tRNA is lethal to *Escherichia coli*. *J. Bacteriol.*, **137**, 694–696.
Menninger,J.R. and Coleman,R.A. (1993) Lincosamide antibiotics stimulate dissociation of peptidyl-tRNA from ribosomes. *Antimicrob. Agents Chemother.*, **37**, 2027–2029.
Nicholls,A. and Honig,B. (1991) A rapid finite difference algorithm utilizing successive over-relaxation to solve the Poisson–Boltzmann equation. *J. Comp. Chem.*, **12**, 435–445.
Nicholls,A., Sharp,K.A. and Honig,B. (1991) Protein folding and association: insights from the interfacial and thermodynamic properties of hydrocarbons. *Proteins*, **11**, 281–286.
Otwinowski,Z. (1991) Maximum likelihood refinement of heavy atom parameters. In Wolf,W., Evans,P.R. and Leslie,A.G.W. (eds), *Isomorphous Replacement and Anomalous Scattering*. Science and Engineering Research Council, Warrington, UK, pp. 80–86.
Sayers,J.R., Schmidt,W. and Eckstein,F. (1988) 5′-3′ Exonucleases in phosphorothioate-based oligonucleotide-directed mutagenesis. *Nucleic Acids. Res.*, **16**, 791–802.
Schmitt,E., Fromant,M., Plateau,P., Mechulam,Y. and Blanquet,S. (1997) Crystallization and preliminary X-ray analysis of *Escherichia coli* peptidyl-tRNA hydrolase. *Proteins*, **28**, 135–136.
Schulman,L. and Pelka,H. (1975) The structural basis for the resistance of *Escherichia coli* formylmethionyl transfer ribonucleic acid to cleavage by *Escherichia coli* peptidyl transfer ribonucleic acid hydrolase. *J. Biol. Chem.*, **250**, 542–547.
Shiloach,J., Bauer,S., De Groot,N. and Lapidot,Y. (1975a) The influence of the peptide chain length on the activity of peptidyl-tRNA hydrolase from *E.coli*. *Nucleic Acids Res.*, **2**, 1941–1950.
Shiloach,J., Lapidot,Y., de Groot,N., Sprinzl,M. and Cramer,F. (1975b) The specificity of peptidyl-tRNA hydrolase from *E.coli*. *FEBS Lett.*, **57**, 130–133.

Received on April 2, 1997; revised on May 9, 1997